Hot Spots and Hot Moments of Nitrogen in a Riparian Corridor

Dipankar Dwivedi[1], Bhavna Arora[1], Carl I. Steefel[1], Baptiste Dafflon[2], and Roelof Versteeg[3]

[1] Energy Geosciences Division, Lawrence Berkeley National Laboratory, Berkeley, CA, USA, [2] Climate and Ecosystem Sciences, Lawrence Berkeley National Laboratory, Berkeley, CA, USA, [3] Subsurface Insights, LLC, Hanover, NH, USA

Correspondence to: D. Dwivedi, DDwivedi@lbl.gov

Abstract

We use 3-D high-resolution reactive transport modeling to investigate whether the spatial distribution of organic-carbon-rich and chemically reduced sediments located in the riparian zone and temporal variability in groundwater flow direction impact the formation and distribution of nitrogen hot spots (regions that exhibit higher reaction rates when compared to other locations nearby) and hot moments (times that exhibit high reaction rates as compared to longer intervening time periods) within the Rifle floodplain in Colorado. Groundwater flows primarily toward the Colorado River from the floodplain but changes direction at times of high river stage. The result is that oxic river water infiltrates the Rifle floodplain during these relatively short-term events. Simulation results indicate that episodic rainfall in the summer season leads to the formation of nitrogen hot moments associated with Colorado River rise and resulting river infiltration into the floodplain. The results further demonstrate that the naturally reduced zones (NRZs) present in sediments of the Rifle floodplain have a higher potential for nitrate removal, approximately 70% greater than non-NRZs for typical hydrological conditions. During river water infiltration, nitrate reduction capacity remains the same within the NRZs, however, these conditions impact non-NRZs to a greater extent (approximately 95% less nitrate removal). Model simulations indicate chemolithoautotrophs are primarily responsible for the removal of nitrate in the Rifle floodplain. These nitrogen hot spots and hot moments are sustained by microbial respiration and the chemolithoautotrophic oxidation of reduced minerals in the riparian zone.

Plain Language Summary

Riverine floodplains play a significant role in the cycling of nitrogen. Reliable predictions of nitrogen dynamics in the floodplain and its export to the river depend on accurate representation of hydrologic flow paths and biogeochemical processes in the subsurface. The objective of this study was to quantify the transport and distribution of nitrogen at a floodplain site in Rifle, CO, using a high-resolution, 3-D flow and reactive transport model. Groundwater flows primarily toward the Colorado River from the floodplain but changes direction occasionally. The simulations demonstrate that nitrogen hot spots are both flow-related and microbially driven in the Rifle floodplain. Overall, 3-D simulations were able to capture the significant

spatial and temporal variability associated with nitrogen fluxes in the floodplain environment.

1 Introduction

Biogeochemical hot spots are regions with disproportionally high reaction rates relative to the surrounding spatial locations, while hot moments are short periods of time manifesting high reaction rates relative to longer intervening time periods. These hot spots and hot moments together affect ecosystem processes and are indeed “ecosystem control points” as suggested by Bernhardt et al. (2017). To investigate linked hydrological and biogeochemical processes, an improved understanding of the controls on biogeochemical hot spots and how they occur as hot moments in natural systems is required.

Biogeochemical hot spots and hot moments play a crucial role in the cycling and transport of metals and nutrients into the river system (Arora et al., 2016b; Bernhardt et al., 2017; Dwivedi & Mohanty, 2016; Harms & Grimm, 2008; McClain et al., 2003). The formation of hot spots and hot moments in riverine systems can be attributed to several causes. A statistical study conducted to analyze biogeochemical hot spots in a streambed showed that the formation of various hot spots was related to the juxtaposition of oxic and anoxic conditions, although these hot spots did not occur simply because of surface water and groundwater (SW-GW) mixing (Lautz & Fanelli, 2008). Another study identified geochemical hot moments in a riverine floodplain as being transport dominated (associated with hydrologic variations) or biogeochemically driven (associated with lithologic heterogeneity, microbial characteristics, etc.) depending on groundwater residence time using wavelet and entropy approaches (Arora et al., 2016a). Although the importance of hot spots and hot moments has been widely recognized in the literature (e.g., Pinay et al., 2015; Vidon & Hill, 2004), most studies have focused on the identification of hot spots and hot moments using statistical techniques and have not analyzed them with physically based modeling approaches.

Relatively, few studies have incorporated hot spots and/or hot moments in numerical models to quantify their aggregated effects on biogeochemical processes at floodplain and riverine scales. Gu et al. (2012) explored biogeochemical hot moments induced by stream fluctuations using a two-dimensional, variably saturated, and reactive transport model. Similarly, Briggs et al. (2014) investigated how hot moments of nitrate production are linked with residence time using one-dimensional conduction-advection-dispersion models. Despite the fact that the data needs are greater than those for hot spots, hot moments have been better represented in modeling studies. In contrast, hot spots are tractable to measure, yet they are not adequately represented in modeling studies because they pose considerable challenges (Groffman et al., 2009). First, the knowledge of the underlying processes that produce hot spots is insufficient. Second, computationally

demanding, high-resolution, fully coupled variably saturated flow and reactive transport models are required if the underlying processes are to be fully represented. In most cases, one-dimensional or two-dimensional flow models are inadequate to capture the spatial patterns of hot spot formation resulting from local variations in microtopography or flow fields. For example, Frei et al. (2012) performed modeling of hot spot formation and demonstrated that they result from spatial variability in soil characteristics, as well as from temporal variability of biogeochemical activity. However, they assumed that there was no interaction between different flow paths, thereby neglecting the potential effects of fluid mixing on the biogeochemistry. This is a particular problem to the extent that mixing between oxic and reduced waters is neglected. We hypothesize that the representation of hydrological and biogeochemical processes in a fully coupled (potentially 3-D) modeling framework will make it possible to simulate explicitly the formation of hot spots and hot moments.

To understand this concept that coupled transient hydrologic processes and spatially distributed biogeochemical activity contribute to spatiotemporal variability in nitrogen dynamics, we investigate how nitrogen hot spots are localized and how hot moments recur within the Rifle floodplain site located in Colorado. The Rifle site is a former uranium mill tailings remedial action site located on the floodplain of the Colorado River. As is typical for floodplain environments, the deposition of organic matter has resulted in the presence of locally, fine-grained, chemically reduced zones within the Rifle site, also referred to as naturally reduced zones (NRZs) (Arora et al., 2016b; Campbell et al., 2012; Janot et al., 2016). Because these NRZs occur primarily next to the stream bank, they affect processes within the riparian zone. Simulating their spatial distribution presents a unique opportunity to critically evaluate their role in the formation and distribution of nitrogen hot spots and hot moments across the site.

Previous modeling studies of the Rifle floodplain have focused on the biogeochemical impacts of water table rise events. For example, Arora et al. (2016b) investigated the release of carbon dioxide from the subsurface via different reactions including heterotrophic and chemolithoautotrophic pathways. They focused specifically on how NRZs, water table variations, and temperature gradients impact subsurface carbon dynamics along a 2-D transect of the Rifle site. Recently, Yabusaki et al. (2017) conducted a three-dimensional modeling study and compared the biogeochemical response (variations in dissolved oxygen, U(VI), and Fe) across NRZ and non-NRZs of the Rifle floodplain specifically targeting the 2014 water table peaking event. Although Yabusaki et al. (2017) incorporated nitrogen biogeochemistry in their study, they did not incorporate nitrification processes explicitly in their reaction network and focused instead on the reductive pathways (see supporting information Table SI-3, Yabusaki et al., 2017). Nitrification can be significant for nitrogen dynamics, particularly when oxic river water or rain water infiltrate, changing the redox state. Further, these nitrogen dynamics

are particularly important for the mobilization of contaminants (e.g., uranium) from the sediments to the river depending on how fast nitrate is consumed (Bone et al., 2017). To the authors' knowledge, the impact of flow reversal associated with the incursion of Colorado River water into the Rifle floodplain and riparian zone interactions on nitrogen dynamics at the Rifle site have not been explored to date. The present study explicitly represents oxidative-reductive pathways of nitrogen biogeochemistry and examines the effect of the influx of river water on biogeochemical processes. Our specific objectives are to assess how this dynamic hydrologic cycle impacts hot spots and hot moments of nitrogen and to investigate the role of naturally reduced zones, if any, on nitrogen dynamics at the site. We also quantify the effects of flow reversal and various reaction pathways on nitrogen dynamics in both NRZs and non-NRZs. To evaluate the dynamic groundwater flow field and linked hydrologic and biogeochemical processes responsible for producing hot spots and hot moments, we integrate a biotic and abiotic reaction network modified from previous modeling studies of the Rifle floodplain site into PFLOTRAN (Hammond et al., 2014), an open source, three-dimensional, reactive flow, and transport simulator. Using these software tools in the context of a fully coupled, high-resolution flow, transport, and biogeochemical reaction simulator allows us to improve our understanding of nitrogen dynamics within a riverine corridor.

2 Methodology and Model Inputs

2.1 Site Description

The Rifle site was formerly a uranium and vanadium ore-processing facility that operated from 1924 through 1958 (Figure 1). These ore-processing operations resulted in the accumulation of a large volume of mill tailings at the site, which were subsequently removed in 1996 as part of the U.S. Department of Energy cleanup efforts (DOE, 1999). However, groundwater beneath the site has remained contaminated with uranium and other radionuclides, albeit at a low level (<3.2 μM; Fox et al., 2012; Shiel et al., 2013; Williams et al., 2013; Yabusaki et al., 2017).

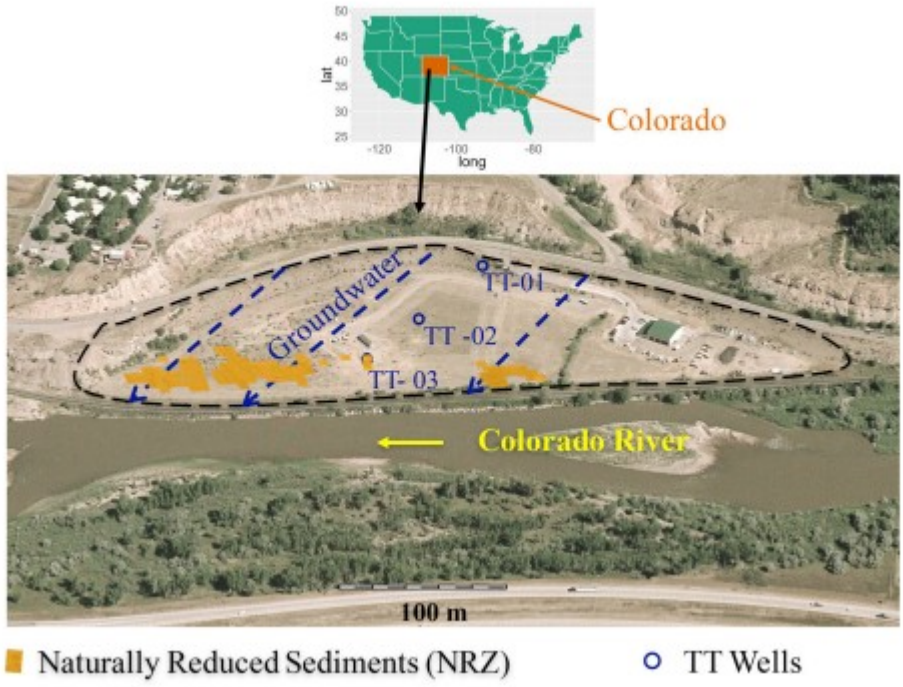

Figure 1

Rifle floodplain is located in western Colorado. Previous studies have identified naturally reduced zones (NRZs; shown in orange) in the saturated alluvium using induced polarization imaging (see, Wainwright et al., 2016). NRZs are linked with elevated organic carbon, Fe(II), sulfide, and U(IV).

Comprehensive descriptions of the site hydrogeology have been presented elsewhere (Anderson et al., 2003; Vrionis et al., 2005; Williams et al., 2011). In brief, the local aquifer consists of Quaternary floodplain deposits that overly the relatively impermeable Wasatch formation (DOE, 1999). The floodplain deposits consist of predominantly loamy soil with unconsolidated gravel and cobbles that are interspersed with fine-grained silt and clay and locally organic-rich sediments (Bao et al., 2014; Campbell et al., 2012). Groundwater at the site is shallow (about 3.5 m below ground surface) and generally flows southwest to the river (Fang et al., 2009; Yabusaki et al., 2011).

Minerals reported in the aquifer sediments include quartz, calcite, clays, and iron-bearing minerals, such as goethite, magnetite, and hematite (Campbell et al., 2012). An abundance of framboidal pyrite has also been reported in NRZ sediments, which comprise 10% of the aquifer volume and are located primarily in the riparian zone (roughly paralleling the Colorado River; Campbell et al., 2012; Qafoku et al., 2009, 2014).

NRZ sediments are associated primarily with elevated concentrations of natural organic matter, Fe(II), nonvolatile sulfides, and uranium (Bargar et al., 2011; Janot et al., 2016). Several studies have noted that the physical properties and biogeochemical characteristics of these sediments are

significantly different from those of nonreduced aquifer sediments. Jewell et al. (2016) suggested that the NRZs are associated with the presence and activity of chemolithoautotrophic bacteria (*Gallionellaceae* and *Sulfurimonas denitrificans*) responsible for the cycling of C, N, Fe, and S. Similarly, Arora et al. (2016b) showed that higher CO_2concentrations were observed above reduced zones as compared to nonreduced zones, suggesting enhanced biogeochemical activity. Arora et al. (2016b) also found that the incorporation of chemolithoautotrophic pathways in model simulations was necessary to reproduce these locally observed CO_2 trends.

The primary monitoring well network used for the current study was installed in 2013. A detailed description of the borehole instrumentation and field sampling protocol is provided in Tokunaga et al. (2016) and Williams et al. (2011). Briefly, instrumentation including tensiometers and soil water and gas samplers were installed at various depths in the vadose zone for sampling. Separate multilevel boreholes were installed for groundwater monitoring and sampling. The groundwater sampling wells accessed three distinct depths near the capillary fringe zone, 1 m below the water table, and the deep aquifer region (Tokunaga et al., 2016). Apart from gas samplers, similar instrumentation sets were used for groundwater sampling wells. Geochemical sampling and measurement methods for chloride, nitrate, and other relevant species are described in Williams et al. (2011).

2.2 Biogeochemical Reaction Network

The biogeochemical reaction network used here is based on previously published flow and reactive transport modeling studies of the Rifle floodplain site (Arora et al., 2016b). The present study expands on the previous work by explicitly addressing vadose zone measurements and processes related to nitrogen biogeochemistry across the entire floodplain. In addition, the biogeochemical reaction network is applied throughout the model domain, although the distinct behaviors are differentiated based on the local abundance or concentration within NRZ and non-NRZ regions.

Following past site investigations (Arora et al., 2016b; Druhan et al., 2012; Li et al., 2009; Yabusaki et al., 2017), key processes included in the reaction network are the degradation of organic carbon through sequential heterotrophic pathways, chemolithoautrophic oxidation of Fe(II) and S^{-2}, and consideration of spatially distinct pools of Fe and S minerals within NRZ and non-NRZ regions. As such, the reaction network explicitly accounts for microbial community dynamics considered relevant at the site (e.g., Anantharaman et al., 2016; Jewell et al., 2016).

As with previous modeling studies (Arora et al., 2016b; Yabusaki et al., 2017), a single solid phase carbon source (SOM) is considered in the reaction network. The solid organic matter (SOM) undergoes acetogenesis to produce dissolved organic carbon (acetate) according to (Table 1)

$$C_6H_{10}O_5 + 2.5H_2O \rightarrow 3CH_3COO^- + 3H^+ \quad (1)$$

Table 1
Microbially Mediated Redox Reactions and Their Parameters Considered in the Simulations

Reaction stoichiometry	Thermodynamic parameters log K (25°C)[a]	Kinetic parameters			
		μ_{max} (/s)	K_S (mol/L)	K_{TEA} (mol/L)	K_I (mol/L)
Redox reactions with heterotrophic pathways					
$CH_3COO^- + 2O_2 \rightarrow 2HCO_3^- + H^+$	146.76	5.0×10^{-12} [b]		2.4×10^{-5} [c]	
$CH_3COO^- + 4NO_3^- \rightarrow 2HCO_3^- + 4NO_2^- + H^+$	89.04	2.0×10^{-10} [d]		1.1×10^{-4} [c]	$K_{I,O2} = 1.6 \times 10^{-8}$ [e]
$CH_3COO^- + 2.667NO_2^- + 1.667H^+ \rightarrow 2HCO_3^- + 1.334N_2 + 1.334H_2O$	200.52	3.0×10^{-8} [b]		1.1×10^{-4} [c]	$K_{I,O2} = 1.6 \times 10^{-8}$ [e]
$NH_3(aq) + 2O_2 \rightarrow NO_3^- + H_2O + H^+$	62.23	5.3×10^{-4} [b]	1.5×10^{-5} [f]	2.4×10^{-5} [c]	
$CH_3COO^- + 8Fe^{+3} + 4H_2O \rightarrow 8Fe^{+2} + 2HCO_3^- + 9H^+$	79.0	1.0×10^{-13} [b]			$K_{I,O2} = 1.6 \times 10^{-8}$ [e] $K_{I,NO3} = 1.0 \times 10^{-7}$
$CH_3COO^- + SO_4^{-2} \rightarrow 2HCO_3^- + HS^-$	8.40	3.0×10^{-12} [b]	1.0×10^{-3} [g]		$K_{I,O2} = 1.6 \times 10^{-8}$ [e] $K_{I,NO3} = 1.0 \times 10^{-7}$ $K_{I,Fe} = 1.0 \times 10^{-12}$
Redox reactions with chemolithoautotrophic pathways					
$Fe^{+2} + 0.25O_2 + H^+ \rightarrow Fe^{+3} + 0.5H_2O$	8.47	5.3×10^{-11} [b]	1.0×10^{-5} [h]	2.4×10^{-5} [c]	
$0.5HS^- + O_2 \rightarrow 0.5H^+ + 0.5SO_4^{-2}$	68.90	2.4×10^{-8} [i]	1.0×10^{-5} [j]	2.4×10^{-5} [c]	
$Fe^{+2} + 0.2NO_3^- + 1.2H^+ \rightarrow Fe^{+3} + 0.1N_2 + 0.6H_2O$	−7.32	7.0×10^{-8} [k]	1.0×10^{-5} [h]	1.1×10^{-4} [c]	$K_{I,O2} = 1.6 \times 10^{-8}$ [e]
$HS^- + 1.6NO_3^- + 0.6H^+ \rightarrow SO_4^{-2} + 0.8N_2 + 0.8H_2O$	11.52	7.0×10^{-8} [k]	1.0×10^{-5} [f]	1.1×10^{-4} [c]	$K_{I,O2} = 1.6 \times 10^{-8}$ [e]

[a]Calculated from log *K* values for half redox reactions reported by (Morel & Hering, 1993).
[b]Calibrated.
[c]Maggi et al. (2008).
[d]Parkhurst and Appelo (1999).
[e]Widdowson et al. (1988).
[f]Wu et al. (2011).
[g]Li et al. (2010).
[h]Mayer et al. (2002).
[i]Luther et al. (2011).
[j]Handley et al. (2013).
[k]Palmer et al. (2010).

The heterotrophic decomposition of acetate is represented by overall reactions for oxic respiration, denitrification, sulfate reduction, and iron reduction. The rates of these reactions are modeled using single Michaelis-Menten kinetics (Table 1):

$$R_s = \mu_{max} \frac{C_S}{K_S + C_S} \frac{C_{TEA}}{K_{TEA} + C_{TEA}} \frac{K_I}{K_I + C_I} \quad (2)$$

where μ_{max} is the maximum rate of reaction; C_S, C_{TEA}, and C_I are the substrate, electron acceptor, and inhibitor concentrations, respectively; K_S and K_{TEA} are the corresponding half-saturation constants for the substrate and terminal electron acceptors (TEAs); and K_I is the inhibition constant. The inhibition terms in equation 2 simulate the sequential utilization of electron acceptors by impeding lower energy-yielding redox reactions when higher energy-yielding electron acceptors are present (e.g., Baedecker & Back, 1979; Hunter et al., 1998). In addition to the heterotrophic reactions involving acetate, chemolithoautotrophic oxidation of Fe^{+2} and HS^- are included in the simulations. To account for nitrogen cycling processes relevant to the site, nitrification of ammonium to nitrate is also considered in this study. The corresponding thermodynamic and kinetic parameters used in the reactive transport model are given in Table 1.

The biotic reaction network, including microbial consortium biodegradation kinetics, is coupled to a multicomponent inorganic reaction system that is based on a separate input thermodynamic database in which redox reactions are not coupled. In this approach, therefore, redox reactions between

compounds of differing redox state are considered only through microbially mediated reactions, allowing for redox disequilibrium to develop (or not) depending on the kinetics. The inorganic reaction processes included in this study are aqueous speciation and mineral precipitation and dissolution reactions. The reaction network that is simulated includes 19 primary species (H_2O, H^+, , HS^-, Al^{+3}, Ca^{+2}, Cl^-, Fe^{+2}, Fe^{+3}, K^+, Mg^{+2}, Na^+, N_2(aq), , , , SiO_2(aq), and acetate). In addition to SOM, four minerals are considered in the model: goethite, pyrite, siderite, and calcite. In contrast to previous site investigations, a spatial conditioning of the mineralogical properties (Fe(II) minerals) associated with the NRZ distribution at the site was carried out based on information from surface geophysics and mineralogical analyses (Campbell et al., 2012; Wainwright et al., 2016; Table 2).

Table 2
Initial Mineral Volume Fractions Considered in the Simulations

Mineral	Specific surface area ($m^2_{mineral}\ m^{-3}_{mineral}$)[a]	Initial volume fraction in NRZ regions	Initial volume fraction in non-NRZ regions
Goethite	60,000	1.2×10^{-3} [b]	2.4×10^{-3} [b]
Calcite	60,000	0.01[c]	0.01[c]
Siderite	60,000	4.09×10^{-3} [d]	0.0
Pyrite	60,000	3.6×10^{-5} [e]	0.0
SOM	1.13×10^{5} [f]	0.0626	0.0626

[a]Specific surface area is calculated assuming 100 μm spherical grains unless otherwise noted.
[b]Based on hydroxylamine-extractable Fe(III) content in fine-grained (<2 mm) Rifle sediments from both NRZ and non-NRZ regions (Campbell et al., 2012; Li et al., 2010).
[c]Assumed low value from visual observation of calcite in sediments.
[d]Based on 0.5 *M* HCl Fe(II) content in fine-grained (<2 mm) Rifle sediments (Campbell et al., 2012) yielding a value largely dominating the amount of Fe(II) sulfide in the NRZ sediment (see footnote e).
[e]Based on 7×10^{-7} mol/g acid volatile sulfide content in fine-grained (<2 mm) NRZ sediments (Campbell et al., 2012).
[f]Based on the smallest particle size fraction (53 μm) with reported organic matter content in Rifle sediments (Campbell et al., 2012).

All mineral precipitation and dissolution reactions are described using Transition State Theory (or TST) type rate laws:

$$R_m = \left(k_{neutral} + k_{H^+}[a_{H^+}] + \Sigma k_j \prod_i [a_{ij}]\right)(1 - Q_m/Keq_m) \quad (3)$$

where $k_{neutral}$, , and k_j are rate constants for neutral, acid, or additional (jth) reaction mechanism, respectively; a_{ij} is the activity of the ith aqueous species in the jth reaction; and Q_m is the ion activity product of the mth mineral phase, and Keq is its corresponding equilibrium constant (Table 2). Reaction stoichiometry and kinetic parameters associated with mineral precipitation and dissolution considered in this study are summarized in supporting information Table S1. Other relevant parameters are listed in Table 2.

2.3 Numerical Model

A 3-D coupled unsaturated-saturated flow and biogeochemical reactive transport model of the Rifle site was developed using the reactive transport software package PFLOTRAN (Hammond et al., 2014). The model domain captures the Rifle floodplain geometry and is set up as 310 m by 830 m by 60 m in *X*, *Y*, and *Z* directions (Figures 2 and 3). The model domain was uniformly discretized with 6.1 m horizontal and 0.25 m vertical resolution using a structured grid. A maximum time step of 1,800 s was used.

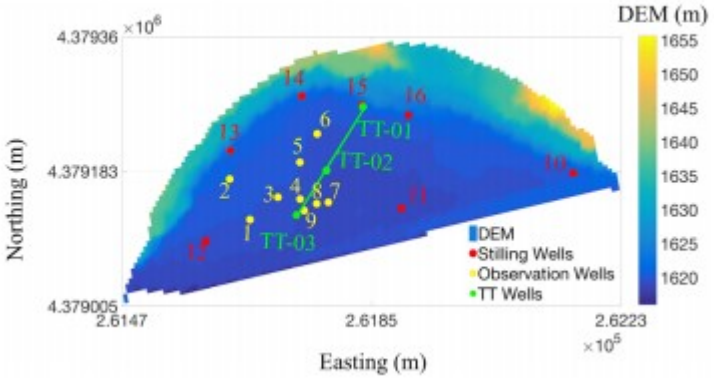

Figure 2

Digital Elevation Model (DEM) of the Rifle floodplain shows that the maximum elevation difference is approximately 50 m. North American Vertical Datum of 1988 (NAVD88) was used for projecting the DEM data. Stilling wells (SY) within the floodplain were used to measure groundwater levels and to provide the basis for the dynamic hydrostatic boundary condition in the three-dimensional model. Different wells are named as follows: 1(FP-103), 2(LR02), 3(M15), 4(X2), 5(655), 6(FP102), 7(LQ102), 8(U01), 9(CD02), 10(SY-07), 11(SY-304), 12(SY-06), 13(SY-04), 14(SY-02), 15(SY-08), and 16(SY-01).

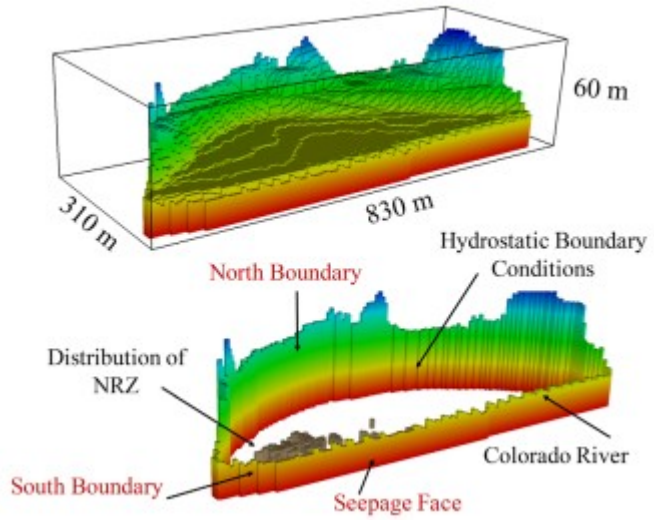

Figure 3

The modeling domain in PFLOTRAN was 310 m by 830 m by 60 m. Naturally reduced zones (NRZs) are located in the sediments on the downstream side of the Colorado River. The Colorado River was assigned as a seepage face, while the north boundary was assigned as a dynamic hydrostatic boundary condition.

The Darcy-Richards equation was used to model water flow under variably saturated conditions. As with previous modeling studies (e.g., Arora et al., 2016b), the fill and alluvium stratigraphic units were represented in the model and the average hydrological properties of the fill and alluvium were estimated using pedotransfer functions from textural data of sediments from the site (Tokunaga et al., 2016). These values are summarized in Table 3. An effective diffusion coefficient of 1.5×10^{-9} m^2 s^{-1} was used in the simulations. The geochemical reaction network as described in section 2.2 was integrated into PFLOTRAN for reactive transport simulations.

Table 3
Average Material Properties for Fill and Alluvium Used in the Simulations (From Tokunaga et al., 2016*)*

Hydrostratigraphic unit	Porosity	Permeability (m^2)	van Genuchten parameter, α (kg^{-1} m s^2)	van Genuchten parameter, m	Residual liquid saturation, S_r
Fill	0.21	4.52×10^{-12}	5.07×10^{-4}	0.18	0.07
Alluvium	0.20	9.67×10^{-12}	8.46×10^{-4}	0.31	0.13

2.4 Initial and Boundary Conditions

The transient Colorado River stage was applied as a seepage face boundary on the south side of the model domain (Figure 3). An arch-shaped physical boundary on the north side (referred to as the north boundary, Figure 3) was set with a dynamic hydrostatic condition that was allowed to vary over the course of the year depending on the well data.

Time-varying water table elevations were projected onto the north boundary cell by cell based on daily water level data (Figure 4). River stage data were also projected onto the river boundary cell by cell based on daily measurements. No-flow boundary conditions were imposed on the lower boundary. Time-varying recharge from rain was applied as the top boundary condition. Daily rainfall data were obtained from the weather station located in the Rifle floodplain (https://wfsfa-data.lbl.gov/portal/html/dataAccess.shtml#). The initial flow condition was a hydrostatic pressure distribution, where the water elevation was set at an 8.0 m depth below the land surface. The model was run for several years, after which nearly dynamic equilibrium conditions were achieved.

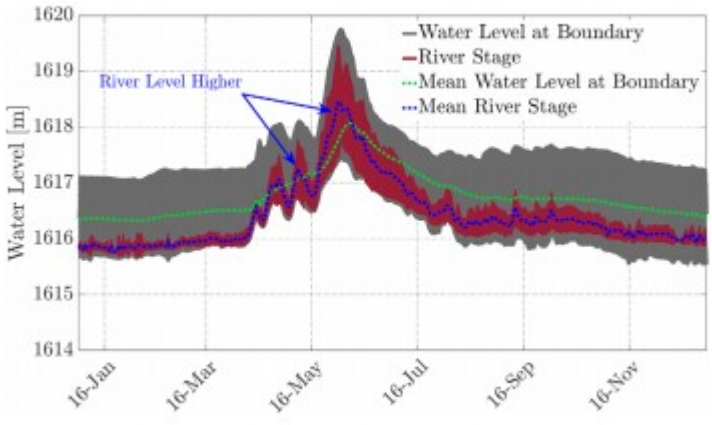

Figure 4

Water levels at the north boundary and river stage data show that groundwater flow direction is from the north boundary to the river through most of the year. However, the river stage is higher than the water levels along the north boundary between mid-April and June, thus reversing the direction of groundwater during this period. NAVD88 datum was used for river stage data and water level elevations.

Following the conceptual model described above, fixed concentrations of dissolved species were applied at the north boundary of the model (Table 4). The fixed water composition at the upgradient boundary was taken as that measured in well TT-01 and was considered representative of oxic recharge from the north boundary. Rain water composition applied at the top model boundary is based on data from National Atmospheric Deposition Program (http://nadp.sws.uiuc.edu/). The river water composition applied at the south boundary is based on water quality data from U.S. Geological Survey (http://nwis.waterdata.usgs.gov/).

Table 4
Initial and Boundary Conditions Used in the Model

Analyte	North recharge boundary condition and initial condition for non-NRZ locations[a]	Initial conditions for NRZ locations[b]	South recharge boundary condition	Top boundary condition
pH[c]	7.01[d]	6.98[d]	8.3	5.44
Acetate	1.00×10^{-10} [e]	9.94×10^{-4}		
Al	3.48×10^{-6}	9.74×10^{-10}		
Ca	5.59×10^{-3}	4.48×10^{-3}	9.04×10^{-4}	4.43×10^{-6}
Cl	6.08×10^{-3}	2.57×10^{-3}	1.52×10^{-3}	1.16×10^{-6}
Fe (II)	7.49×10^{-5}	7.85×10^{-5}		
Fe (III)	6.15×10^{-13} [f]	6.28×10^{-13} [f]		
HCO_3	8.24×10^{-3}	9.53×10^{-3}	1.53×10^{-3}	
K	3.48×10^{-4}	2.00×10^{-4}	4.26×10^{-5}	5.39×10^{-7}
Mg	6.16×10^{-3}	4.06×10^{-3}	2.91×10^{-4}	7.84×10^{-7}
Na	1.25×10^{-2}	7.56×10^{-3}	1.65×10^{-3}	1.31×10^{-6}
N_2 (aq)	1.00×10^{-10} [e]	1.00×10^{-10} [e]		
NH_3 (aq)	6.67×10^{-6}	2.22×10^{-4}	1.17×10^{-6}	7.12×10^{-6}
NO_2	1.05×10^{-6}	1.00×10^{-10} [e]		
NO_3	2.31×10^{-5}	1.00×10^{-10} [e]	2.02×10^{-5}	7.46×10^{-6}
O_2 (aq)	7.83×10^{-6}	1.00×10^{-10} [e]	5.14×10^{-4}	3.23×10^{-4} [g]
S(–2)	1.07×10^{-10} [h]	1.07×10^{-10} [h]		
SiO_2 (aq)	3.30×10^{-4}	4.04×10^{-4}		
SO_4	1.18×10^{-2} [i]	6.94×10^{-3} [i]	4.75×10^{-4}	2.73×10^{-6}
$P_{CO2\ (12°C)}$	0.028 bar	0.028 bar		

[a]Measured pore water concentration in well TT-01, unless indicated otherwise.
[b]Measured pore water concentration in well TT-03, unless indicated otherwise.
[c]pH units.
[d]Equilibrated with calcite.
[e]Low assumed value (below detection).
[f]Equilibrated with goethite.
[g]Fixed by P_{O2} (g) of $10^{-0.7}$ bar.
[h]Equilibrated with pyrite.
[i]Adjusted for charge balance. The blank cells represent low concentrations of different species, e.g., 1.00×10^{-20} *M*.

The initial conditions were based on the spatial NRZ distribution (Figures 1 and 3) such that the groundwater composition at well TT-03 was used to represent the suboxic, reducing conditions at all NRZ locations (Table 4). In contrast, the groundwater composition at well TT-01 was chosen as initial condition at the remaining spatial locations (Table 4). It should be pointed out that given the several years spin-up of the model prior to actual simulations, the initial groundwater compositions are flushed (or reacted) out of the system. The solid phase constituents of the sediments throughout the entire domain were also populated in a similar manner such that NRZ locations were set with an initial mineral composition representative of reduced sediments (Table 2). For example, both NRZs and non-NRZs included calcite, goethite, and SOM in their sediments. However, NRZs differed from non-NRZs because of the presence of higher organic matter and Fe(II) content, while iron oxyhydroxides were higher in the non-NRZs (Qafoku et al., 2014). Figure 3 shows locations of the NRZ in the modeling domain.

2.5 Model Analysis

We simulated a fully coupled biogeochemical system in the Rifle floodplain from 1 January to 31 December 2014. To carry out the simulations, we made use of several observation wells in the floodplain that monitored water levels. We tested our model for flow simulations in seven wells scattered across the floodplain as shown in Figure 2. To test our model for the reactive transport simulations, we primarily used three wells (TT-01, TT-02, and TT-03) because these wells were monitored regularly for various geochemical species and provided local nitrogen data across NRZ and non-NRZ locations. TT-03 is located within the NRZ (Figures 1 and 2). The TT transect is considered representative of both vertical and lateral heterogeneity, by including the fill and alluvium layers as well as NRZ and non-NRZ locations, expected at the extensively studied site (e.g., Arora et al., 2016b; Tokunaga et al., 2016; Wainwright et al., 2016). Further, we used data from multiple depths of the TT wells to demonstrate that the model can reasonably capture observed nitrogen trends within the vadose zone and groundwater. Although most of the nitrogen data are distributed along what is essentially a 2-D transect (by design of the original field investigators), some geochemical data were available at locations other than the TT transect (e.g., dissolved oxygen at SY-08 and nitrite concentration at FP wells). Moreover, the 3-D modeling framework accounts for the systematic integration of information from geophysical imaging (e.g., NRZ and non-NRZ locations; Figures 1 and 3), mineralogical analyses (sediments samples across the floodplain, see section 2.1), and monitored water levels (SY wells and observations wells; as shown in Figure 2), and water quality parameters in other wells (e.g., FP-102, FP-103, U-01, SY-08, and TT wells across the full (3-D) width of the floodplain. Here the intent is to use a floodplain-wide modeling framework to better understand and interpret the interplay of subsurface properties, biogeochemical processes, and hydrologic conditions leading to the observed nitrogen behavior.

3 Results and Discussion

3.1 Simulations of Saturation Levels in the Vadose Zone for the Rifle Site

Figure 5 shows simulated and observed saturation levels at well TT-03 as a function of depth on 25 March 2014. Consistent with field observations, simulated saturation levels show a modest decline in the fill layer and a steep decline in the alluvial layer, thus highlighting the contrast in porous media properties between these two layers. These results, including the slight underestimation of the saturation levels within the shallow fill layer, are consistent with previous site investigations (Arora et al., 2016b). Figure 5 also demonstrates that the vadose zone extends up to 4.25 m at well TT-03 at certain times of the year.

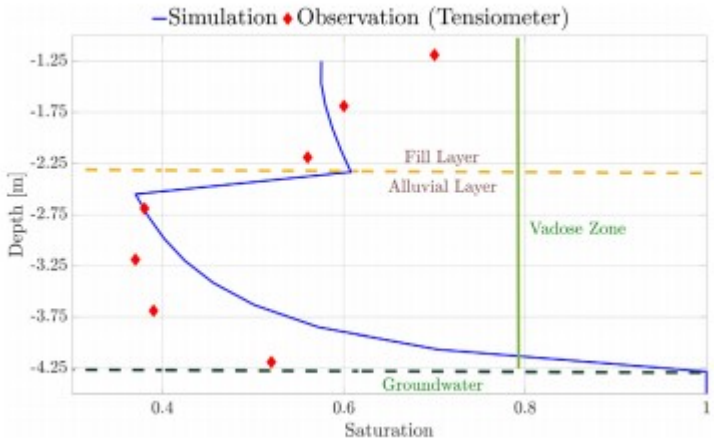

Figure 5

Simulated and observed saturation levels in well TT-03.

3.2 Simulations of Water Levels for the Rifle Site

Figure 6 shows simulated and observed water levels for an entire year (1 January to 31 December 2014) in various observation wells across the Rifle floodplain. Simulated water levels closely matched the observed values. The model was able to capture the hydrologic variability across these wells. Both the simulated and observed profiles demonstrate that the water table rises in late spring to early summer as a result of snowmelt.

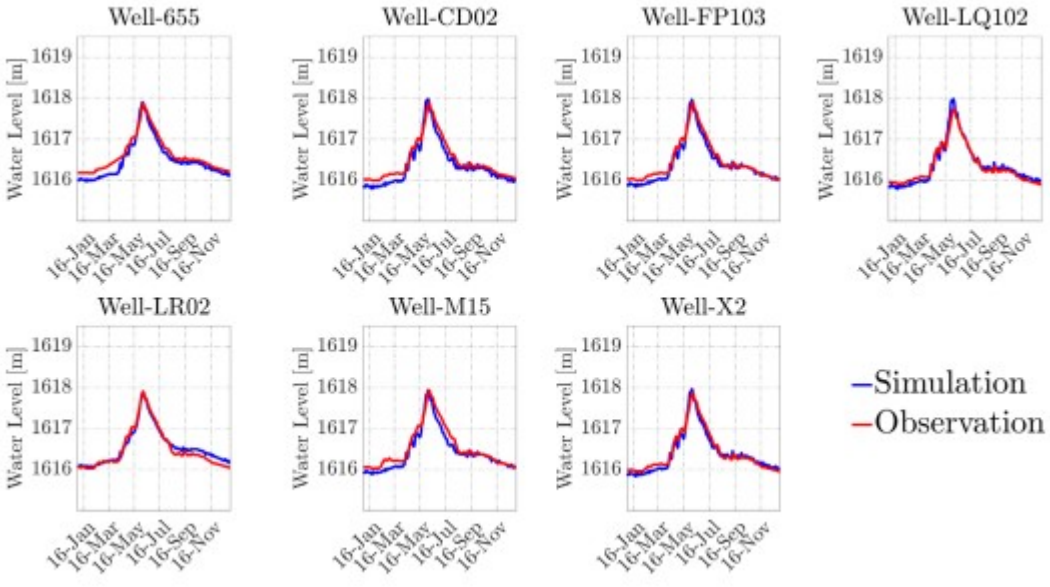

Figure 6

Simulated and observed water levels across the floodplain in different observation wells.

Past studies (e.g., DOE, 1999; Williams et al., 2011) have suggested that groundwater flow is toward the Colorado River throughout the year along most of the riverbank. Flow simulations in our study demonstrate that

groundwater typically follows the topographic gradient, and water generally flows toward the Colorado River. However, our modeling results show a reversal in groundwater flow direction between mid-April and June 2014 (Figure 7). As shown in Figure 7, snapshots of flow paths at 100, 150, 200, and 250 days show the reversal in groundwater flow direction over the entire boundary on Day 150 (30 May). Overall, groundwater flow reversals are consistent with times when the river stage data exceed groundwater elevations (e.g., between mid-April and June) as shown in Figure 4. This water flow into the Rifle aquifer leads to the formation of dynamic redox conditions in the subsurface, which subsequently contributes to the evolution of geochemical hot spots and hot moments.

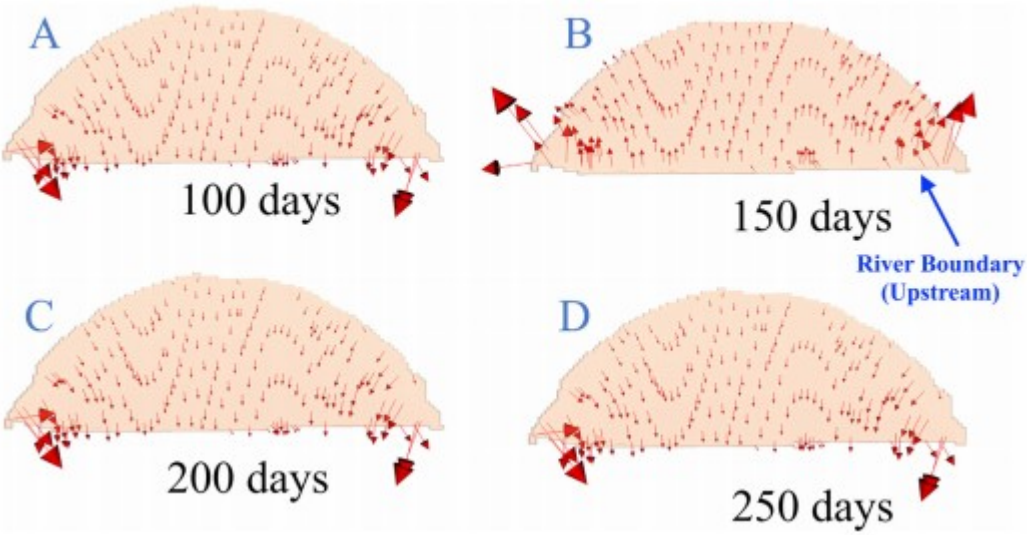

Figure 7

Map view of flow paths are shown at 5.0 m depth in groundwater. 100, 150, 200, and 250 days correspond to 10 April, 30 May, 19 July, and 7 September in 2014, respectively. Flow paths show a reversal in groundwater flow direction on 150th day. There are multiple instances between mid-April and June when groundwater flow direction is from the Colorado River to the Rifle floodplain.

3.3 Simulations of Chloride for the Rifle Site

To further understand the dynamic hydrologic behavior at the site, we simulated chloride concentrations and then compared these to observations from TT wells in the floodplain (Figure 8). Different depths were chosen as observation points so as to represent distinct processes (e.g., precipitation inputs versus river water infiltration) in the vadose zone and groundwater. Note that observed chloride concentrations do not show significant variability along the TT transect in the vadose zone or groundwater, except in well TT-03 that showed slightly lower chloride concentration in comparison to wells TT-01 and TT-02. This lower chloride concentration in well TT-03 can be attributed to dilution resulting from groundwater flow reversal, since river water has a slightly lower chloride concentration as compared to the background aquifer (Table 4). Furthermore, Figure 8 demonstrates that

model predictions matched observed chloride concentrations reasonably well with an average bias of −1 m*M* in the vadose zone and 0.5 m*M* in groundwater. Here bias is defined as the mean of the difference between simulated and observed concentrations. Overall, the model underpredicted chloride concentrations in the vadose zone, while groundwater chloride concentrations were overpredicted. In general, the model performed better in the groundwater than in the vadose zone.

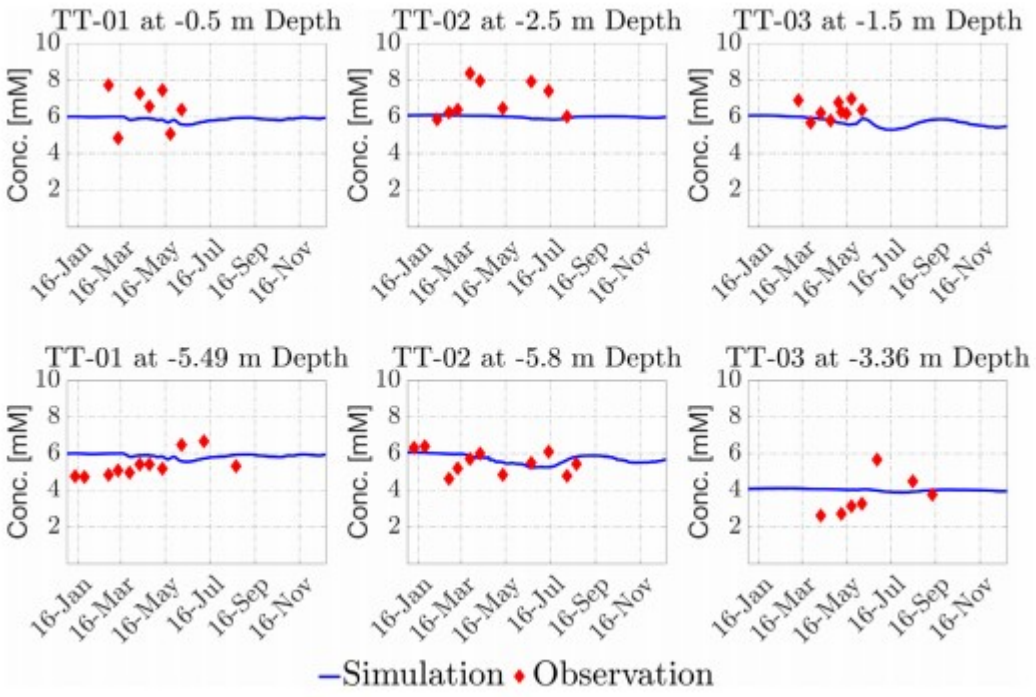

Figure 8

Simulated and observed chloride concentrations at different depths in TT wells.

3.4 Simulations of Nitrate and Nitrite for the Rifle Site

Simulated and observed profiles of nitrate within the vadose zone (TT-01: 1.5 m; TT-02: 2.5 m; and TT-03: 1.5 and 3.14 m) and groundwater (TT-01: 5.49 and 7.02 m; TT-02: 4.58 and 5.8 m; and TT-03: 5.95 m) are shown in Figure 9. Note that both observations and simulation results suggest that more variability is associated with nitrate concentrations in wells TT-02 and TT-03 than in well TT-01 in the vadose zone, particularly during the late spring season (Figure 9). In particular, both TT-02 and TT-03 wells show higher nitrate concentration from late April to early May, which coincides with the snowmelt period. However, observed nitrate concentration in well TT-02 indicates a slower rate of decline (extending from late April to early October) as compared to TT-03, where nitrate concentration first increases from January to early May, then steeply declines in mid-May, followed by an increase until late June, and a corresponding decrease. The high nitrate concentration observed at different times in well TT-03 appears to coincide with the early snowmelt period and multiple rainfall events. Consistent with

observations, model predictions were able to capture these temporal trends in vadose zone nitrate concentrations across the TT transect reasonably well. In contrast, Figure 9 indicates that observed groundwater nitrate concentrations show higher variability in well TT-01, with higher nitrate concentration observed from late February to early April, as compared to low concentration in well TT-03. In fact, observed and simulated groundwater nitrate concentrations in well TT-03 show consistently low values throughout the year. These differences in temporal trends across the TT transect wells can be explained by the fact that wells TT-01 and TT-02 are located in non-NRZs, whereas well TT-03 is located within the NRZ. Note that model simulations were able to capture this more rapid removal of nitrate in well TT-03 as a result of the chemolithoautotrophic consumption by microbes (explained in more detail below). In contrast, nitrate concentrations in wells TT-01 and TT-02 are primarily controlled by the influx of the boundary water, which is determined by the combination of snowmelt and rainfall events and heterotrophic consumption.

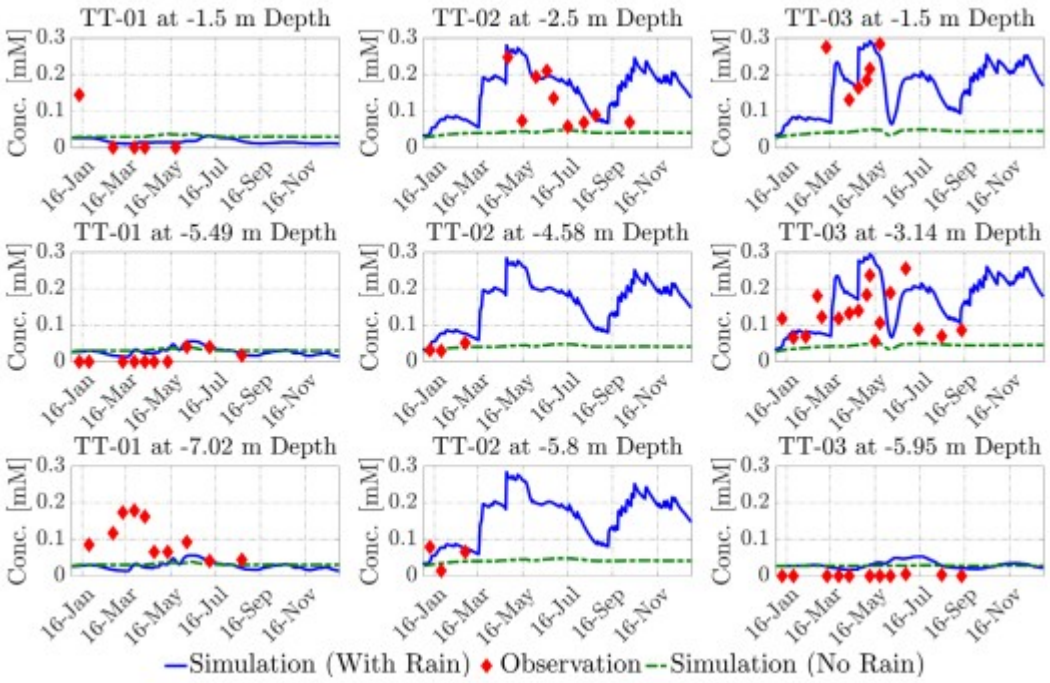

Figure 9

Simulated and observed nitrate concentrations at different depths in TT wells. The average water table depth is approximately 3.5 m below the land surface.

Figure 10 shows simulated and observed groundwater nitrite concentration in wells TT-02, TT-03, FP-102, and FP-103. Simulated nitrite concentrations closely matched the observed values in all wells except well TT-02. In particular, the simulated results underpredicted observed nitrite concentrations in well TT-02.

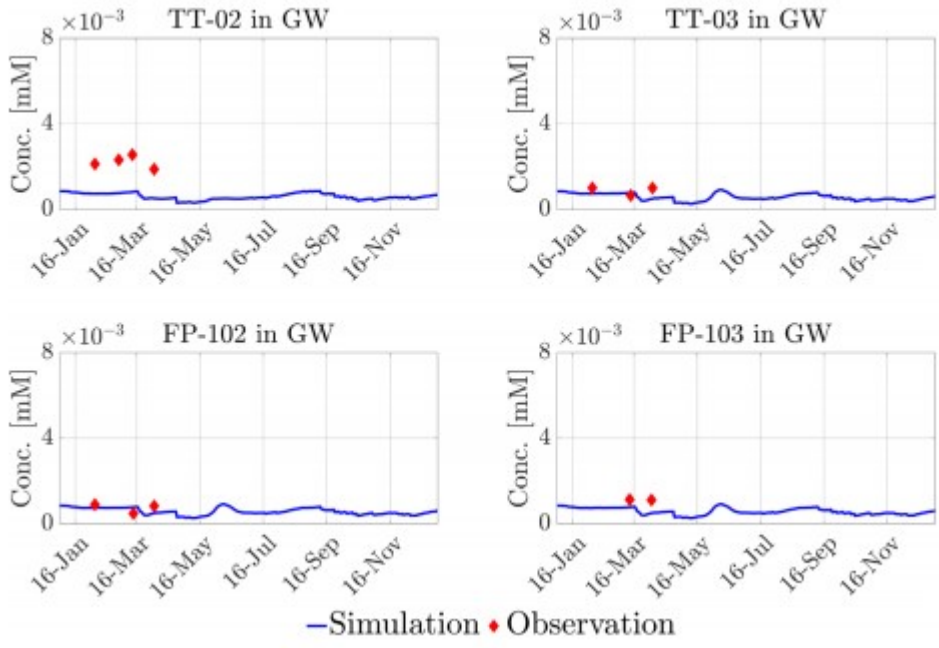

Figure 10

Simulated and observed nitrite concentrations in groundwater at TT and FP wells.

The steady source of nitrate into the floodplain occurred as a result of subsurface groundwater flow. Nitrate may be transported into the floodplain from either the hillslope or the river. In addition, the decomposition of organic matter from the floodplain soils may also contribute to nitrate levels through nitrification, a microbially mediated oxidation of ammonium ion to nitrate (Gomez-Velez et al., 2015). Therefore, nitrification could be an important process in the vadose zone, primarily when oxygen-rich rain water flows into the subsurface environment. Nitrate can subsequently be transformed into a variety of reduced nitrogen species through denitrification. Eventually, nitrate can be converted to dinitrogen species (referred to as nitrogen hereafter) through a series of microbially mediated redox reactions. In the process, microbes consume dissolved organic carbon (DOC) Dwivedi et al. (2017) and use nitrate and nitrite as terminal electron acceptors. Denitrification is limited by the available DOC and is favored under anoxic conditions (Gu et al., 2012; Maggi et al., 2008; Rosswall, 1982), although there is no such limitation considered in these simulations.

The SW-GW transition zone of the Rifle floodplain experiences infiltration and exfiltration events as a result of river stage changes and variable hydrological conditions in the subsurface, as described in section 3.2. Through most of the year, the Colorado River gains water. However, as previously discussed, river water moves into the floodplain at multiple instances (e.g., 21–28 April, 6–9 May, and 20 May to 8 June 2014) for short durations and subsequently recedes. Although flow reversal events are not prolonged (approximately 1–2 days), the SW-GW transition zone undergoes changes in redox conditions. Redox conditions are altered because of

infiltration of oxic and higher pH of river water. Moreover, river water, which has nitrate values similar to the north boundary water (Table 4), also contributes additional nitrate to groundwater during infiltration.

Consider the high nitrate values observed in groundwater during the late spring season in well TT-03 (Figure 9). One possibility is that nitrate-rich water entered the floodplain from the river due to flow reversal in the riparian corridor of the Rifle floodplain. This hypothesis is further supported using model simulations (see section 3.5). Well TT-03 is near the river, and it changes from anoxic to suboxic during this period due to river water infiltration (Figures 11 and 12). During this short-lived flow reversal, the nitrate also moves into the floodplain from the river water. However, TT-03 quickly becomes anoxic, after which the nitrate is transformed into nitrogen through biotic pathways. The fact that TT-03 is located within an NRZ and is consequently rich in reduced minerals like pyrite is an important reason why O_2 and nitrate are transformed so quickly. Several studies have shown that chemolithoautotrophic pathways (the reduction of iron and sulfide minerals by oxygen and nitrate) are important within the NRZs at the Rifle site (e.g., Arora et al., 2016b; Jewell et al., 2016). Therefore, well TT-03, because of the abundance of reduced reactive species there, acts as a hot spot of nitrogen. Together, these results suggest that the causes for hot spots of nitrogen in the vicinity of TT-03 seem to be both flow related and microbially driven. These results further suggest that hot spots do not occur because of simple fluid mixing, i.e., as the result of nitrate moving into the floodplain with river water. Rather, these hot spots occur because of flow reversal that introduces oxygenated, nitrate-rich water into the NRZ, followed by a sequence of heterotrophic and chemolithoautotrophic reaction pathways involving reduced minerals (principally sulfides; see Tables 1 and 2).

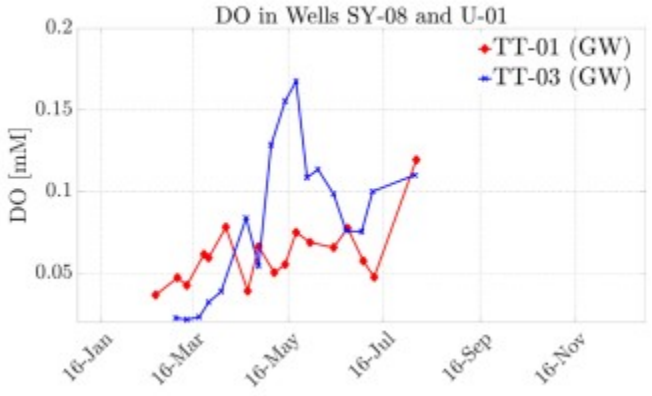

Figure 11

Observed DO concentrations in groundwater at wells SY-08 (close to TT-01) and U-01 (close to TT-03). Oxygen levels suggest that river water infiltration results in oxic conditions at TT-03.

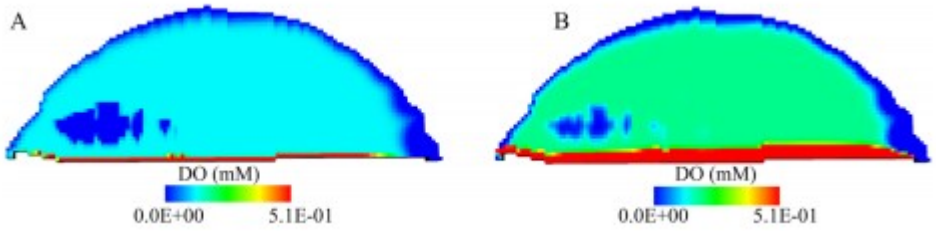

Figure 12

Snapshots of simulated dissolved oxygen at 5.0 m depth in groundwater on 100 ((a) before the flow reversal; 10 April 2014) and 150 ((b) during the flow reversal; 19 July 2014) days. Map view of dissolved oxygen shows the change in the redox state due to flow reversal.

Now consider the high nitrate values observed in the vadose zone of wells TT-02 and TT-03 (Figure 9). High nitrate values in the vadose zone could occur when ammonia is released from the decomposition of organic matter in soils. We hypothesize that rainfall can lead to the formation of hot moments of nitrogen species in the Rifle subsurface because of nitrification resulting from the percolation of oxic water. The Rifle floodplain received 34 cm of rainfall in 2014, and 20% of the precipitation occurred between mid-April and June. As can be seen in Figure 9, average nitrate levels were 0.1 m*M* in TT wells, but nitrate levels were higher than the average in the vadose zone between late April and early May. Thus, we argue that high nitrate levels in wells TT-02 and TT-03 were primarily due to nitrification resulting from rain water percolation between late April and early May. After May and June, nitrate levels decline in wells TT-02 and TT-03, but the decline was sharper in the case of well TT-03. The sharper decline can again be attributed to well TT-03 being located within the NRZ, where multiple biotic pathways (heterotrophic + chemolithoautotrophic) are associated with nitrate consumption. To confirm this hypothesis, we used nitrate-to-chloride ratios to distinguish different sources contributing to vadose zone porewaters. Native groundwater at the Rifle site had a low nitrate-to-chloride ratio (approximately 10^{-4}) whereas river water had a higher ratio of 0.01. In contrast, rainwater had a ratio of 6.43. Figure 13 shows that vadose zone samples from wells TT-02 and TT-03 had higher nitrate-to-chloride ratios than other vadose zone and groundwater samples from the site, suggesting that a different source—most likely nitrification from rain water percolation—could be an important source of nitrate in the NRZs.

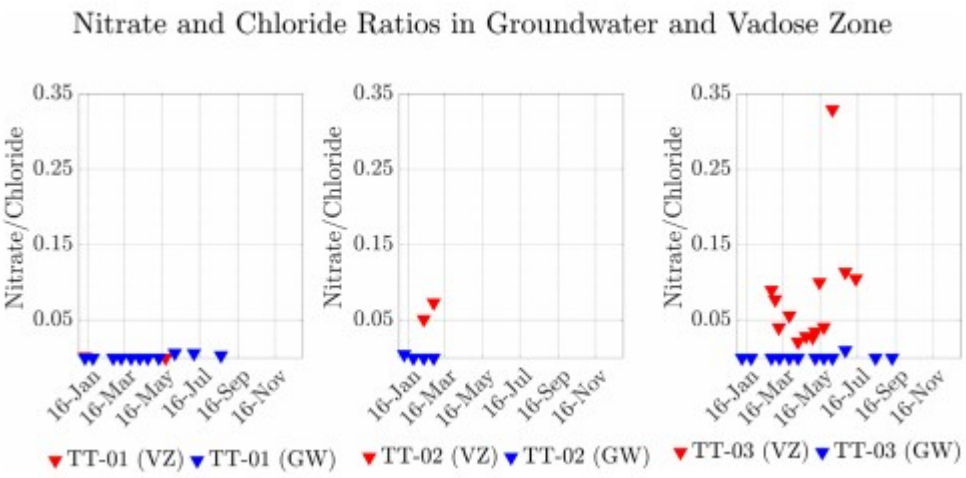

Figure 13

Nitrate and chloride ratios suggest the vadose zone contributes to nitrate levels.

To further demonstrate the importance of ammonia released from organic-carbon-rich sediments during rainfall events, we performed an additional simulation that did not consider rainfall (Figure 9). Figure 9 shows that simulations without rainfall (green line) failed to capture nitrate variability in TT wells. Nitrification contributed up to 35% (TT-01), 67% (TT-02), and 48% (TT-03) of nitrate levels in groundwater. Taken together, these results suggest that (1) short-lived flow reversal and (2) episodic rainfall events lead to the formation of hot spots and hot moments of nitrate in the riparian corridor.

3.5 Hot Spots and Hot Moments of Nitrogen at the Rifle Site

To highlight key processes that trigger the formation of hot spots and hot moments in the Rifle floodplain, we present simulated results of nitrate transformation at different times in the year to capture transient hydrologic and periodic oxic and anoxic conditions. Figure 14shows eight snapshots of simulation results of nitrate and nitrogen at 5 m depth below the ground surface. These snapshots represent the spatial distribution of nitrogen species at different times (100, 150, 200, and 250 days).

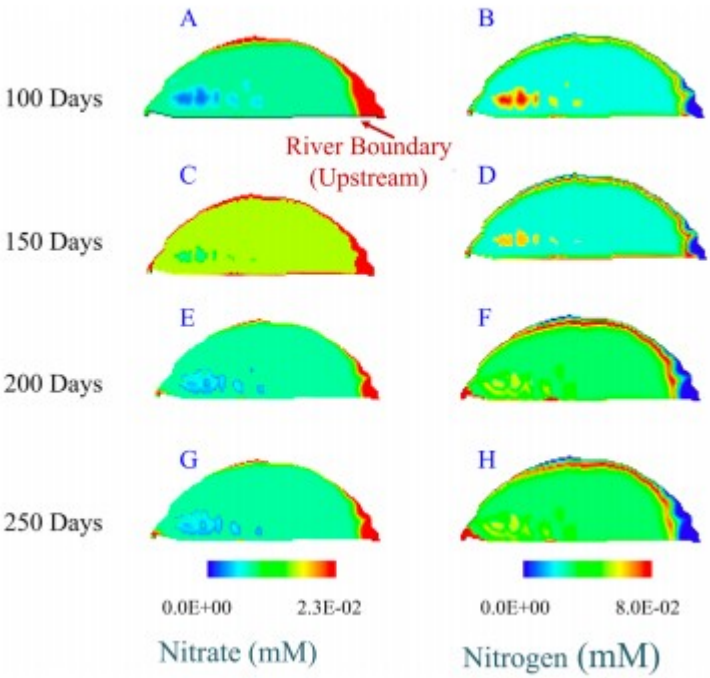

Figure 14

Simulated nitrate and nitrogen concentrations at 5.0 m depth in the Rifle floodplain at various times during the simulation period. 100, 150, 200, and 250 days correspond to 10 April, 30 May, 19 July, and 7 September in 2014, respectively.

Snapshots of nitrogen transformation at 100th day (10 April) show a high concentration (represented by red color) of nitrate and nitrogen near the north boundary and slightly away from the north boundary, respectively. Nitrogen concentration is high whereas nitrate is low in the NRZs. Note that 3 days of rain events preceded the 100th day simulation, and precipitation totaled to 1 cm at that time. This implies that nitrate enters the floodplain primarily through subsurface water flow from the hillslope (approximately 78%), and partly through nitrification in the vadose zone (22%; Figure 14A). At this time, the flow direction of groundwater is toward the Colorado River (Figure 7A), so nitrate is partly exported to the river (approximately 18%), and the rest is lost through denitrification (82%).

Snapshots of simulated nitrogen species at 150th day (30 May) show relatively homogenous nitrate and nitrogen levels across the floodplain. However, high concentrations of nitrate and nitrogen along the north and south boundaries can be noted (Figures 14C and 14D). These snapshots coincide with times when river water moves into the floodplain (Figure 7B). During this period, nitrate is not exported into the river, remaining instead within the floodplain.

Snapshots of simulated nitrogen species at 200th day (19 July) show high nitrate and nitrogen along the north boundary as well as a high

concentration of nitrogen extending from the NRZ to the river (Figures 14E and 14F). This is a relatively dry period, and the river gains water from the Rifle groundwater (Figure 7C). Nitrate is exported to the river, and high levels of nitrate along the north boundary result due to the influx from the hillslope. However, high levels of nitrogen occur in the center of the modeling domain and extend through the river boundary. This shows that NRZ again plays an important role in the formation of hot spots of nitrogen insofar as they transform nitrate into nitrogen quickly.

Snapshots of nitrogen species at 250th day (7 September) show similar spatial patterns of nitrate the snapshots of 200th day. High nitrate levels along the north boundary are again due to the influx from the hillslope (Figures 14G and 14H). Nitrate is exported to the river and partly lost through denitrification. However, nitrogen is also exported to the Colorado River because of the hydrologic flow paths (Figure 7D), and there are no significant additional sources of nitrate (e.g., from the river or through nitrification in the vadose zone) at this time (Figure 14H).

It can also be seen from Figure 14 that nitrate and nitrogen show significant spatial variability across the floodplain, particularly in the vicinity of the NRZs. Water levels did not show this level of spatial variability across wells, and each well had concurrent rising and falling limbs (Figure 6). However, a distinct pattern of nitrogen species is apparent across the floodplain. Based on these observations, we conclude that these spatial patterns are predominantly driven by the presence of reduced sediments and partly by hydrologic flow paths. These results also demonstrate that the 3-D time-resolved model is able to capture the variable redox conditions resulting from river stage changes and transient hydrological conditions. An important implication of this spatiotemporal variability at the site contributes to highly variable fluxes of nitrogen species to the river.

4 Quantifying Effects of NRZ and Non-NRZ on Nitrogen Dynamics Under Different Hydrological and Biogeochemical Conditions

To better understand nitrogen dynamics in the Rifle floodplain, which has spatially distributed NRZs and experiences short-duration flow reversal, we conducted a sensitivity analysis. In particular, we analyzed the sensitivity of nitrogen to flow reversal and microbial pathways considering (a) only heterotrophic and (b) all (heterotrophic + chemolithoautotrophic) reactions for both NRZs and non-NRZs. We also varied rates of reaction by an order of ±1 from the baseline rates for each scenario. For these analyses, all (heterotrophic + chemolithoautotrophic) reactions with rates as described in Table 1 were used as the baseline scenario. We compared changes in nitrogen concentrations for each scenario with respect to nitrogen concentration in non-NRZs with the baseline parameters. Note that the production of nitrogen is directly linked to the removal of nitrate from the floodplain. In other words, the higher the nitrogen production, the higher is the nitrate removal potential for that particular scenario.

These scenarios simulate different hydrological and biogeochemical conditions across the floodplain throughout the year (Figure 15). For example, the first (all reactions and typical flow direction) and second scenarios (only heterotrophic reactions and typical flow direction) represent general hydrological conditions in the aquifer and quantify contributions of heterotrophs and chemolithoautotrophs on nitrate removal, whereas the third (all reactions and flow reversal) and fourth (only heterotrophic reactions and flow reversal) scenarios describe hydrologic conditions when oxic river water infiltrates and changes redox conditions in the aquifer. The third and fourth scenarios also apportion contributions of heterotrophs and chemolithoautotrophs on nitrate removal. Together, these scenarios demonstrate how nitrate removal potential varies across NRZ and non-NRZ sediments. Figure 15 presents the percent change in nitrogen production across these scenarios as compared to the baseline simulation. It is clear from Figure 15 that NRZs produce more nitrogen (approximately 70%) than non-NRZs. In other words, NRZs show a higher nitrate removal potential than non-NRZs. Flow reversal leads to a lower production of nitrogen (approximately 95%) in the non-NRZ whereas the NRZ remains unaffected by the flow reversal as far as the production of nitrogen is concerned. The results also show that chemolithoautotrophs contribute predominantly to nitrate removal during typical and flow reversal conditions. Chemolithoautotrophic pathways reduce approximately twice as much nitrate in sediments as heterotrophic pathways because chemolithoautotrophs oxidize sulfide and iron, whereas heterotrophs remove nitrate only by oxidizing dissolved organic carbon. These reactions are only inhibited by oxygen; therefore, if chemolithoautotrophs are present, they are likely to reduce more nitrate—approximately twice as much as that reduced by heterotrophs.

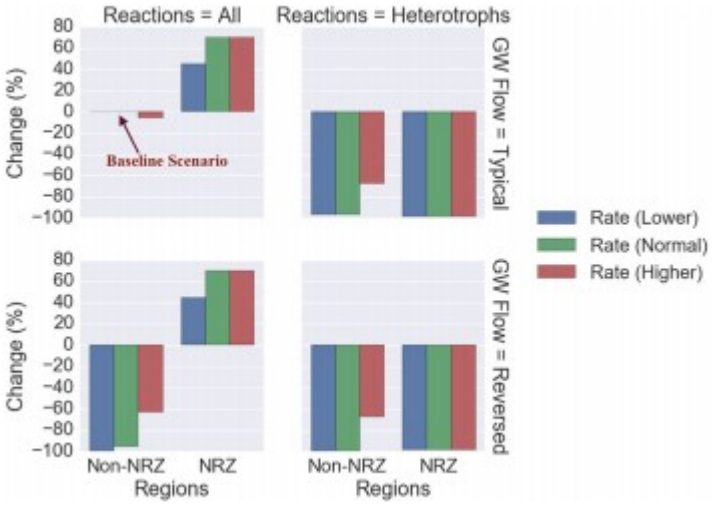

Figure 15

Sensitivity of nitrogen to flow reversal and microbial pathways in NRZ and non-NRZ.

Flow reversal has a significant influence on nitrate reduction carried out by chemolithoautotrophic pathways in non-NRZs but only a modest effect (<10%) in NRZs. Moreover, flow reversal does not have any significant influence on nitrate reduction carried out by heterotrophic pathways in either NRZs (<1%) or non-NRZs (<10%). Together, flow reversal influences nitrate removal or nitrogen production in non-NRZs, but not within NRZs. Flow reversal leads to the infiltration of oxic water. Nitrogen production carried out by chemolithoautotrophic and heterotrophic pathways is inhibited by oxygen. Dissolve oxygen is consumed rapidly in NRZs than non-NRZs because of the oxidative dissolution of pyrite in NRZs. Therefore, NRZs do not show significant differences when oxic water enters the floodplain, while in contrast, non-NRZs do not reduce nitrate until the oxygen is consumed.

For each scenario, when we varied rates of all the reactions by an order of ±1 from the baseline rates, higher rates of reactions produced 20%–30% higher nitrogen levels across all scenarios involving non-NRZs. This increase in nitrogen production is linked to the more rapid depletion of oxygen. NRZs do not show any significant differences in nitrogen production regardless of higher or lower rates of reactions since reduced minerals sustain anoxic conditions within the NRZs both during and after the flow reversal events.

5 Conclusions

To understand key processes that produce hot spots and hot moments of nitrogen in a floodplain environment, we developed a high-resolution, three-dimensional subsurface reactive transport model. The model was able to capture the hydrological and biogeochemical variability across the Rifle floodplain. Model simulations suggested that an accurate characterization of hydrological forcing and SW-GW interactions was crucial for predicting hot spots and hot moments of nitrogen at our site. In general, these hot phenomena may be flow related or microbially driven, but hydrologic transients provided conditions that led to the formation of hot spots. At our site, groundwater flow typically follows the topographic gradient moving from the floodplain to the river. The Colorado River is thus a gaining river through most of the year, however, an intermittent groundwater flow reversal because of SW-GW interaction leads to dynamic redox conditions in the riparian corridor. These redox conditions also produced hot spots and hot moments of nitrogen. Moreover, high-intensity, short-duration rainfall in the summer season was found to be a significant driver causing hot spots and hot moments of nitrogen. Sensitivity analyses demonstrated that the NRZs have a higher potential for nitrate removal than the non-NRZs for identical hydrological conditions. However, flow reversal leads to a reduction in nitrate removal (approximately 95% lower) in non-NRZs whereas the NRZ remains unaffected by the influx of the river water.

3-D simulations were useful in capturing the significant spatial and temporal variability associated with nitrogen fluxes in the floodplain environment. In particular, simulation results demonstrated that hot and cold moments of

nitrogen did not coincide in different wells, in contrast to flow hydrographs. This can have significant implications for managing nonpoint sources of contamination, such as abandoned mines or agricultural lands, where sources resulting in high levels of nitrate in drinking water can pose adverse human health effects (Brender et al., 2013; Shaffer et al., 1995).

Although we demonstrated how hot spots form and hot moments recur in a floodplain using examples of nitrogen transformation, this approach should be readily transferable to other riparian corridors. In particular, identifying nitrogen hot moments can help with pollution source analysis and mitigating risks associated with the persistence of nitrate in groundwater (e.g., Dwivedi & Mohanty, 2016). Further, nitrogen hot spots and hot moments may not occur alone; instead, they may occur simultaneously or even trigger the cycling of other nutrients, metals, and contaminants (e.g., Vidon et al., 2008).

Acknowledgments

This material is based on work supported by the Small Business Innovation Research and the Genomes to Watershed Scientific Focus Area at Lawrence Berkeley National Laboratory funded by the U.S. Department of Energy, Office of Science, Office of Biological and Environmental Research under awards DE-SC0009732 and DE-AC02–05CH11231, respectively. This research used resources of the National Energy Research Scientific Computing Center, which is supported by the Office of Science of the U.S. Department of Energy under contract DE-AC02–05CH11231. The data used are listed in the references, tables, and supporting information. The authors thank Nic Spycher at Lawrence Berkeley National Laboratory for his valuable suggestions, which greatly improved this manuscript.

References

Anantharaman, K., Brown, C. T., Hug, L. A., Sharon, I., Castelle, C. J., Probst, A. J., … Banfield, J. F. (2016). Thousands of microbial genomes shed light on interconnected biogeochemical processes in an aquifer system. *Nature Communications*, 7, 1– 11.

Anderson, R. T., Vrionis, H. A., Ortiz-Bernad, I., Resch, C. T., Long, P. E., Dayvault, R., … Lovley, D. R. (2003). Stimulating the in situ activity of geobacter species to remove uranium from the groundwater of a uranium-contaminated aquifer. *Applied and Environmental Microbiology*, 69(10), 5884– 5891. https://doi.org/10.1128/AEM.69.10.5884-5891.2003

Arora, B., Dwivedi, D., Hubbard, S. S., Steefel, C. I., & Williams, K. H. (2016a). Identifying geochemical hot moments and their controls on a contaminated river floodplain system using wavelet and entropy approaches. *Environmental Modelling & Software*, 85, 27– 41. https://doi.org/10.1016/j.envsoft.2016.08.005

Arora, B., Spycher, N. F., Steefel, C. I., Molins, S., Bill, M., Conrad, M. E., … Yabusaki, S. B. (2016b). Influence of hydrological, biogeochemical and temperature transients on subsurface carbon fluxes in a flood plain environment. *Biogeochemistry*, 127(2–3), 367– 396. https://doi.org/10.1007/s10533-016-0186-8

Baedecker, M. J., & Back, W. (1979). Modern marine sediments as a natural analog to the chemically stressed environment of a landfill. *Journal of Hydrology*, 43(1), 393– 414. https://doi.org/10.1016/0022-1694(79)90183-5

Bao, C., Wu, H., Li, L., Long, P. E., Newcomer, D., & Williams, K. H. (2014). Uranium bioreduction rates across scales: Biogeochemical hot moments and hot spots during a biostimulation experiment at Rifle, Colorado. *Environmental Science & Technology*, 48(17), 10116– 10127. https://doi.org/10.1021/es501060d

Bargar, J. R., Campbell, K. M., Stubbs, J. E., Suvorova, E., Williams, K., Lezama-Pacheco, J. S., … Giammar, D. E. (2011). Speciation and dynamics of biologically reduced uranium(IV) in the Old Rifle aquifer. *Abstracts of Papers of the American Chemical Society*, 242.

Bernhardt, E. S., Blaszczak, J. R., Ficken, C. D., Fork, M. L., Kaiser, K. E., & Seybold, E. C. (2017). Control points in ecosystems: Moving beyond the hot spot hot moment concept. *Ecosystems*, 20(4), 665– 682. https://doi.org/10.1007/s10021-016-0103-y

Bone, S. E., Cahill, M. R., Jones, M. E., Fendorf, S., Davis, J., Williams, K. H., & Bargar, J. R. (2017). Oxidative uranium release from anoxic sediments under diffusion-limited conditions. *Environmental Science & Technology*, 51(19), 11039– 11047. https://doi.org/10.1021/acs.est.7b02241

Brender, J. D., Weyer, P. J., Romitti, P. A., Mohanty, B. P., Shinde, M. U., Vuong, A. M., … National Birth Defects Prevention Study. (2013). Prenatal nitrate intake from drinking water and selected birth defects in offspring of participants in the national birth defects prevention study. *Environmental Health Perspectives*, 121(9), 1083– 1089. https://doi.org/10.1289/ehp.1206249

Briggs, M. A., Lautz, L. K., & Hare, D. K. (2014). Residence time control on hot moments of net nitrate production and uptake in the hyporheic zone. *Hydrological Processes*, 28(11), 3741– 3751. https://doi.org/10.1002/hyp.9921

Campbell, K. M. M., Kukkadapu, R. K., Qafoku, N. P., Peacock, A. D., Lesher, E., Williams, K. H., … Long, P. E. (2012). Geochemical, mineralogical and microbiological characteristics of sediment from a naturally reduced zone in a uranium-contaminated aquifer. *Applied Geochemistry*, 27(8), 1499– 1511. https://doi.org/10.1016/j.apgeochem.2012.04.013

DOE. (1999). *Final site observational work plan for the UMTRA Project old Rifle site*. Grand Junction, CO: Author.

Druhan, J. L., Steefel, C. I., Molins, S., Williams, K. H., Conrad, M. E., & Depaolo, D. J. (2012). Timing the onset of sulfate reduction over multiple subsurface acetate amendments by measurement and modeling of sulfur isotope fractionation. *Environmental Science & Technology*, 46, 8895– 8902. https://doi.org/10.1021/es302016p

Dwivedi, D., & Mohanty, B. P. (2016). Hot spots and persistence of nitrate in aquifers across scales. *Entropy*, 18(1), 25. https://doi.org/10.3390/e18010025

Dwivedi, D., Riley, W. J., Torn, M. S., Spycher, N. & Tang, J. Y. (2017). Mineralogy, microbes, transport, and plant-input profiles control vertical distribution and age of soil carbon stocks. *Soil Biology and Biochemistry*, 107, 244– 259. https://doi.org/10.1016/j.soilbio.2016.12.019

Fang, Y., Yabusaki, S. B., Morrison, S. J., Amonette, J. P., & Long, P. E. (2009). Multicomponent reactive transport modeling of uranium bioremediation field experiments. *Geochimica et Cosmochimica Acta*, 73(20), 6029– 6051. https://doi.org/10.1016/j.gca.2009.07.019

Fox, P. M., Davis, J. A., Hay, M. B., Conrad, M. E., Campbell, K. M., Williams, K. H., & Long, P. E. (2012). Rate-limited U(VI) desorption during a small-scale tracer test in a heterogeneous uranium-contaminated aquifer. *Water Resources Research*, 48, W05512. https://doi.org/10.1029/2011WR011472

Frei, S., Knorr, K. H., Peiffer, S., & Fleckenstein, J. H. (2012). Surface micro-topography causes hot spots of biogeochemical activity in wetland systems: A virtual modeling experiment. *Journal of Geophysical Research*, 117, G00N12. https://doi.org/10.1029/2012JG002012

Gomez-Velez, J. D., Harvey, J. W., Cardenas, M. B., & Kiel, B. (2015). Denitrification in the Mississippi River network controlled by flow through river bedforms. *Nature Geoscience*, 8, 1– 8. https://doi.org/10.1038/ngeo2567

Groffman, P. M., Butterbach-Bahl, K., Fulweiler, R. W., Gold, A. J., Morse, J. L., Stander, E. K., … Vidon, P. (2009). Challenges to incorporating spatially and temporally explicit phenomena (hotspots and hot moments) in denitrification models. *Biogeochemistry*, 93(1–2), 49– 77. https://doi.org/10.1007/s10533-008-9277-5

Gu, C., Anderson, W., & Maggi, F. (2012). Riparian biogeochemical hot moments induced by stream fluctuations. *Water Resources Research*, 48, W09546. https://doi.org/10.1029/2011WR011720

Hammond, G. E., Lichtner, P. C., & Mills, R. T. (2014). Evaluating the performance of parallel subsurface simulators: An illustrative example with PFLOTRAN. *Water Resources Research*, 50, 208– 228. https://doi.org/10.1002/2012WR013483

Handley, K. M., VerBerkmoes, N. C., Steefel, C. I., Williams, K. H., Sharon, I., Miller, C. S., … Banfield, J. F. (2013). Biostimulation induces syntrophic

interactions that impact C, S and N cycling in a sediment microbial community. *The ISME Journal*, 7(4), 800– 816. https://doi.org/10.1038/ismej.2012.148

Harms, T. K., & Grimm, N. B. (2008). Hot spots and hot moments of carbon and nitrogen dynamics in a semiarid riparian zone. *Journal of Geophysical Research*, 113, G01020. https://doi.org/10.1029/2007JG000588

Hunter, K. S., Wang, Y., & Van Cappellen, P. (1998). Kinetic modeling of microbially-driven redox chemistry of subsurface environments: Coupling transport, microbial metabolism and geochemistry. *Journal of Hydrology*, 209(1–4), 53– 80. https://doi.org/10.1016/S0022-1694(98)00157-7

Janot, N., Lezama Pacheco, J. S., Pham, D. Q., O'Brien, T. M., Hausladen, D., Noël, V., … Bargar, J. R. (2016). Physico-chemical heterogeneity of organic-rich sediments in the Rifle aquifer, CO: Impact on uranium biogeochemistry. *Environmental Science & Technology*, 50(1), 46– 53. https://doi.org/10.1021/acs.est.5b03208

Jewell, T. N., Karaoz, U., Brodie, E. L., Williams, K. H., & Beller, H. R. (2016). Metatranscriptomic evidence of pervasive and diverse chemolithoautotrophy relevant to C, S, N and Fe cycling in a shallow alluvial aquifer, *The ISME Journal*, 10(9), 2106– 2117.

Lautz, L. K., & Fanelli, R. M. (2008). Seasonal biogeochemical hotspots in the streambed around restoration structures. *Biogeochemistry*, 91(1), 85– 104. https://doi.org/10.1007/s10533-008-9235-2

Li, L., Steefel, C. I., Kowalsky, M. B., Englert, A., & Hubbard, S. S. (2010). Effects of physical and geochemical heterogeneities on mineral transformation and biomass accumulation during biostimulation experiments at Rifle, Colorado. *Journal of Contaminant Hydrology*, 112(1–4), 45– 63. https://doi.org/10.1016/j.jconhyd.2009.10.006

Li, L., Steefel, C. I., Williams, K. H., Wilkins, M. J., & Hubbard, S. S. (2009). Mineral transformation and biomass accumulation associated with uranium bioremediation at Rifle, Colorado. *Environmental Science & Technology*, 43(14), 5429– 5435. https://doi.org/10.1021/es900016v

Luther, G. W., Findlay, A. J., MacDonald, D. J., Owings, S. M., Hanson, T. E., Beinart, R. A., & Girguis, P. R. (2011). Thermodynamics and kinetics of sulfide oxidation by oxygen: A look at inorganically controlled reactions and biologically mediated processes in the environment. *Frontiers in Microbiology*, 2, 62. https://doi.org/10.3389/fmicb.2011.00062

Maggi, F., Gu, C., Riley, W. J., Hornberger, G. M., Venterea, R. T., Xu, T., … Oldenburg, C. M. (2008). A mechanistic treatment of the dominant soil nitrogen cycling processes: Model development, testing, and application. *Journal of Geophysical Research*, 113, G02016. https://doi.org/10.1029/2007JG000578

Mayer, K. U., Frind, E. O., & Blowes, D. W. (2002). Multicomponent reactive transport modeling in variably saturated porous media using a generalized formulation for kinetically controlled reactions. *Water Resources Research*, 38(9), 1174. https://doi.org/10.1029/2001WR000862

McClain, M. E., Boyer, E. W., Dent, C. L., Gergel, S. E., Grimm, N. B., Groffman, P. M., … Pinay, G. (2003). Biogeochemical hot spots and hot moments at the interface of terrestrial and aquatic ecosystems. *Ecosystems*, 6(4), 301– 312. https://doi.org/10.1007/s10021-003-0161-9

Morel, F. M. M., & Hering, J. G. (1993). *Principles and applications of aquatic chemistry*. New York, NY: John Wiley.

Palmer, K., Drake, H. L., & Horn, M. A. (2010). Association of novel and highly diverse acid-tolerant denitrifiers with N_2O fluxes of an acidic fen. *Applied and Environmental Microbiology*, 76(4), 1125– 1134. https://doi.org/10.1128/AEM.02256-09

Parkhurst, D. L., & Appelo, C. A. J. (1999). *User's guide to PHREEQC (version 2): A computer program for speciation, batch-reaction, one-dimensional transport, and inverse geochemical calculations* (Water Resour. Invest. Rep. 99–4259). Denver, CO: Earth Science Information Center, Open-File Reports Section, U.S. Geological Survey.

Pinay, G., Peiffer, S., De Dreuzy, J. R., Krause, S., Hannah, D. M., Fleckenstein, J. H., … Hubert-Moy, L. (2015). Upscaling nitrogen removal capacity from local hotspots to low stream orders' drainage basins. *Ecosystems*, 18(6), 1101– 1120. https://doi.org/10.1007/s10021-015-9878-5

Qafoku, N. P., Gartman, B. N., Kukkadapu, R. K., Arey, B. W., Williams, K. H., Mouser, P. J., … Long, P. E. (2014). Geochemical and mineralogical investigation of uranium in multi-element contaminated, organic-rich subsurface sediment. *Applied Geochemistry*, 42, 77– 85. https://doi.org/10.1016/j.apgeochem.2013.12.001

Qafoku, N. P., Kukkadapu, R. K., McKinley, J. P., Arey, B. W., Kelly, S. D., Wang, C., … Long, P. E. (2009). Uranium in framboidal pyrite from a naturally bioreduced alluvial sediment. *Environmental Science & Technology*, 43(22), 8528– 8534. https://doi.org/10.1021/es9017333

Rosswall, T. (1982). Microbiological regulation of the biogeochemical nitrogen cycle. *Plant and Soil*, 67(1–3), 15– 34. https://doi.org/10.1007/BF02182752

Shaffer, M. J., Wylie, B. K., & Hall, M. D. (1995). Identification and mitigation of nitrate leaching hot spots using NLEAP-GIS technology. *Journal of Contaminant Hydrology*, 20(3–4), 253– 263. https://doi.org/10.1016/0169-7722(95)00072-0

Shiel, A. E., Laubach, P. G., Johnson, T. M., Lundstrom, C. C., Long, P. E., & Williams, K. H. (2013). Measurable changes in $^{238}U/^{235}U$ due to desorption–adsorption of U(VI) from groundwater at the Rifle, Colorado, integrated field

research challenge site. *Environmental Science & Technology*, 47(6), 2535–2541. https://doi.org/10.1021/es303913y

Tokunaga, T. K., Kima, Y., Conrada, M. E., Billa, M., Hobsona, C., Williams, K. H., … Hubbard, S. S. (2016). Deep Vadose zone respiration contributions to carbon dioxide fluxes from a semiarid floodplain. *Vadose Zone Journal*, 15(7). https://doi.org/10.2136/vzj2016.02.0014

Vidon, P., Tedesco, L. P., Wilson, J., Campbell, M. A., Casey, L. R., & Gray, M. (2008). Direct and indirect hydrological controls on *E. coli* concentration and loading in midwestern streams. *Journal of Environmental Quality*, 37(5), 1761– 1768. https://doi.org/10.2134/jeq2007.0311

Vidon, P. G. F., & Hill, A. R. (2004). Landscape controls on nitrate removal in stream riparian zones. *Water Resources Research*, 40, W03201. https://doi.org/10.1029/2003WR002473

Vrionis, H. A., Anderson, R. T., Ortiz-Bernad, I., O'Neill, K. R., Resch, C. T., Peacock, A. D., … Lovley, D. R. (2005). Microbiological and geochemical heterogeneity in an in situ uranium bioremediation field site. *Applied and Environmental Microbiology*, 71, 6308– 6318. https://doi.org/10.1128/AEM.71.10.6308-6318.2005

Wainwright, H. M., Flores Orozco, A., Bücker, M., Dafflon, B., Chen, J., Hubbard, S. S., & Williams, K. H. (2016). Hierarchical Bayesian method for mapping biogeochemical hot spots using induced polarization imaging. *Water Resources Research*, 52, 533– 551. https://doi.org/10.1002/2015WR017763

Widdowson, M. A., Molz, F. J., & Benefield, L. D. (1988). A numerical transport model for oxygen- and nitrate-based respiration linked to substrate and nutrient availability in porous media. *Water Resources Research*, 24(9), 1553– 1565. https://doi.org/10.1029/WR024i009p01553

Williams, K. H., Long, P. E., Davis, J. A., Wilkins, M. J., N'Guessan, A. L., Steefel, C. I., … Lovley, D. R. (2011). Acetate availability and its influence on sustainable bioremediation of uranium-contaminated groundwater. *Geomicrobiology Journal*, 28(5–6), 519– 539. https://doi.org/10.1080/01490451.2010.520074

Williams, K. H., Wilkins, M. J., N'Guessan, A. L., Arey, B., Dodova, E., Dohnalkova, A., … Long, P. E. (2013). Field evidence of selenium bioreduction in a uranium-contaminated aquifer. *Environmental Microbiology Reports*, 5(3), 444– 452. https://doi.org/10.1111/1758-2229.12032

Wu, Y.-S., Di, Y., Kang, Z., & Fakcharoenphol, P. (2011). A multiple-continuum model for simulating single-phase and multiphase flow in naturally fractured vuggy reservoirs. *Journal of Petroleum Science and Engineering*, 78(1), 13–22. https://doi.org/10.1016/j.petrol.2011.05.004

Yabusaki, S., Wilkins, M. J., Fang, Y., Williams, K. H., Arora, B., Bargar, J., … Wainwright, H. M. (2017). Water table dynamics and biogeochemical cycling

in a shallow, variably-saturated floodplain. *Environmental Science & Technology*, 51(6), 3307– 3331. https://doi.org/10.1021/acs.est.6b04873

Yabusaki, S. B., Fang, Y., Williams, K. H., Murray, C. J., Ward, A. L., Dayvault, R. D., … Long, P. E. (2011). Variably saturated flow and multicomponent biogeochemical reactive transport modeling of a uranium bioremediation field experiment. *Journal of Contaminant Hydrology*, 126(3–4), 271– 290. https://doi.org/10.1016/j.jconhyd.2011.09.002